Stochastic Approach to the Study of Atomistic Processes in the Early Stages of Thin-Film Growth. 2. Island Formation

Russell Davidson

GREQAM, 2 Rue de la Charite, 13002 Marseille, France and Department of Economics, Queen's University, Kingston, Ontario K7L 3N6, Canada

John J. Kozak*

Department of Chemistry, Iowa State University, Ames, Iowa 50011

Received: August 29, 1997; In Final Form: April 6, 1998

We draw upon the theoretical methods developed in the preceding contribution to explore different mechanisms of island growth in the initial stages of the development of a thin film. In particular, we study the entropic consequences of assuming different sequences for generating a final nucleation pattern or island morphology on a finite, planar array. Our calculations lead to the conclusion that the most entropically favorable process for island growth is one in which the morphology is generated by a "row-filling" mechanism on a lattice with triangular geometry.

I. Introduction

In their recent review, Zhang and Lagally[1] note the factors surrounding the growth of specific island morphologies. Broadly speaking, there are two classes of shapes, one compact with relatively straight and equiaxed island edges, the second fractal-like, having rough island edges or highly anisotropic shapes. A critical factor in the development of compact islands is the difficulty (or not) of a diffusing adatom crossing the corner of an island at which two edges meet. Presented here is an extension of the theoretical "shorthand" introduced in the previous paper[2] (hereafter referred to as part I), which allows one to examine the statistical factors surrounding the development of different island morphologies by considering explicitly different scenarios for the sequential deposition of adatoms from the vapor phase.

The trapping or immobilization of a randomly diffusing adatom at a particular site can be studied using the theory of finite Markov processes. Consider a random walker which is trapped irreversibly at a site within the boundary of a finite, planar array. As noted in part I, a well-defined relationship exists between the first-order rate constant k_D of such an irreversible diffusion-controlled process, and the average number $\langle n \rangle$ of steps before immobilization of the diffusing adatom on the lattice. Hence, calculations of $\langle n \rangle$ also calibrate the time scale of the underlying process, and we use this relationship later to guide the analysis of the stochastic data generated in this study.

Once the time scale of an initial trapping event has been determined, the diffusion of a second adatom on the same finite, planar array can be studied, but subject to the constraint that once the first adatom has been immobilized at a particular site, that site is inaccessible to a second diffusing adatom (i.e., the site occupied by the first adatom is "blocked".) The $\langle n \rangle_j$ ($j = 2$), corresponding to this second event in a j-stage nucleation process, can be calculated, as can the $\langle n \rangle_j$ for each subsequent stage in the process, all subject to the constraint that, as the island morphology begins to unfold, all sites occupied at that stage of the pattern formation are inaccessible to subsequent diffusing adatoms.

Two features of the above description deserve emphasis. First, as noted in ref 1, as sites become "blocked," the diffusional space accessible to subsequent diffusing adatoms contracts: in fact, on finite planar arrays, not only do subsequent adatoms have available a smaller space within which to diffuse, but they have to negotiate more "obstacles", (i.e., the "blocked" sites). Second, in a j-step deposition process, depending on the symmetry, there are as many as $j!$ different ways in which a given final morphology can be generated (i.e., there are many developing configurations of blocked sites (defining the island morphology) that can lead (eventually) to a given final pattern in the deposition process). Approaches for quantifying the statistical consequences of both of these features will be described in the following sections.

The plan of this paper is the following. In section II we extend the theory developed in the preceding contribution to deal explicitly with the situation where adatoms are sequentially immobilized on the underlying host lattice. Then, in section III we present results on three different scenarios of island growth. In the concluding section IV, we link our stochastic approach to a calculation of the entropic differences among the three nucleation mechanisms considered in this study.

II. Theory for Sequential Traps

Consider a lattice with a single trap. A walker moves over the lattice until being trapped. Next another trap opens, often on an adjoining site, and the (filled) original trap is then blocked. Another walker moves over the modified lattice until it, too, is trapped. The second trap is then blocked and a third opened, and so on, for some predetermined number of traps.

It is convenient to develop an iterative procedure for computing expected walk lengths at the successive stages of the above scheme. We can do this by making use of the results in the previous paper. There, we modeled random walks on lattices as stationary Markov processes on a finite state space. Each point in this state space corresponds either to a lattice

S1089-5647(97)02823-X CCC: $15.00
Published on Web 08/29/1998

site, or, more frequently, to a symmetry class of lattice sites. If a lattice has N states, the properties of a random walk on this lattice are characterized by an $N \times N$ Markov transition matrix $\mathbf{P}$, of which the typical element, p_{ij} say, is the probability, conditional on being in state i, that the next step of the walk goes to state j.

If the lattice has one or more traps, and if any walk ends with probability 1 in one of these traps, then one can form the matrix $\mathbf{\Pi} \equiv (\mathbf{I} - \mathbf{P})^{-1}$, which has the property that its typical element π_{ij} is the expected number of visits to state j of the lattice for a walk that starts in state i.

In the scheme described above, the $\mathbf{P}$ matrix changes in a simple way as each new trap opens and its predecessor is blocked. In the previous paper, we considered each of two operations, first, the opening of a new trap, and, second, the blocking of an existing trap, and derived simple formulas for the corresponding changes to the $\mathbf{\Pi}$ matrix. In this section, we use those results in order to derive the changes to $\mathbf{\Pi}$ when both operations take place.

We number our lattice states in such a way that the trap to be blocked will be indexed by 0, while the trap to be opened will have index 1. The original $\mathbf{P}$ matrix can be written in partitioned form as follows:

$$\mathbf{P} = \begin{bmatrix} 0 & 0 & 0_{(1,N-2)} \\ p_{10} & p_{11} & \mathbf{P}_1 \\ \mathbf{p}_0 & \mathbf{p}_1 & \mathbf{Q} \end{bmatrix}$$

Here $\mathbf{P}_1$ is a $1 \times (N-2)$ row, containing the probabilities of going from state 1 to the states other than 0 or 1, $\mathbf{p}_0$ and $\mathbf{p}_1$ are $(N-2) \times 1$ columns containing the probabilities for going from the states other than 0 or 1 to 0 or 1 respectively, and $\mathbf{Q}$ is an $(N-2) \times (N-2)$ matrix. The whole first row of $\mathbf{P}$ is zero precisely because state 0 is a trap. Similarly, the original $\mathbf{\Pi}$ matrix can be written as

$$\mathbf{\Pi} = \begin{bmatrix} 1 & 0 & 0_{(1,N-2)} \\ 1 & \pi_{11} & \boldsymbol{\rho}_1 \\ \iota_{(N-2,1)} & \boldsymbol{\pi}_1 & \hat{\mathbf{\Pi}} \end{bmatrix}$$

where ι is a column vector with all elements equal to 1. All of the elements of column 0 of $\mathbf{\Pi}$ are 1 because state 0 is the only trap on the lattice: regardless of where a walk starts, it always pays exactly one visit to state 0 and is then trapped. All the elements of row 0, except the 0 element itself, are 0 because, starting from the trap, there is nowhere else to go.

When the new trap opens at state 1, the change to $\mathbf{P}$ can be written as

$$\Delta\mathbf{P} = -\mathbf{e}_1 \begin{bmatrix} p_{10} & p_{11}\, \mathbf{P}_1 \end{bmatrix}$$

where $\mathbf{e}_1$ is an $N \times 1$ vector with all elements zero except that indexed by 1, which equals 1. It is easy to see that $\mathbf{P}' \equiv \mathbf{P} + \Delta\mathbf{P}$ has a row indexed by 1 which is zero: state 1 is indeed a trap. It was shown in the previous paper that $\Delta\mathbf{\Pi}$, the matrix of changes to $\mathbf{\Pi}$ caused by the changes $\Delta\mathbf{P}$, can be written as

$$\Delta\mathbf{\Pi} = -\frac{1}{\pi_{11}} \begin{bmatrix} 0 \\ \pi_{11} \\ \boldsymbol{\pi}_1 \end{bmatrix} \left(\begin{bmatrix} 1 & \pi_{11} & \boldsymbol{\rho}_1 \end{bmatrix} - \mathbf{e}_1^{\tau} \right) \tag{1}$$

At the end of our calculation, we will keep only the rows and columns of $\Delta\mathbf{\Pi}$ after those indexed by 0 and 1, because those rows and columns of the changed $\mathbf{\Pi}$ are trivial. In the meantime, though, we retain everything. We define $\mathbf{\Pi}' \equiv \mathbf{\Pi} + \Delta\mathbf{\Pi}$.

The next step is to block the trapping state 0. This involves changes to $\mathbf{P}'$ as follows:

$$\Delta\mathbf{P}' = \sum_{i \in \mathbf{N}_0} p_{i0} \mathbf{e}_i (\mathbf{e}_i^{\tau} - \mathbf{e}_0^{\tau})$$

Here $\mathbf{N}_0$ denotes the set of states that, according to $\mathbf{\Pi}'$, can communicate directly with state 0 before it is blocked. Note that state 1 cannot belong to $\mathbf{N}_0$, because it is a trap in $\mathbf{P}'$. Note also that the operation of blocking is defined in such a way that any step which, before blocking, would have gone to state 0, now simply stops where it is for one step. If $\mathbf{N}_0$ is empty, this just means that, with the opening of state 1 as a trap, state 0 is inaccessible from any other lattice site, and so no further changes to $\mathbf{\Pi}'$ are needed. Otherwise, let ν_0 be the number of states contained in $\mathbf{N}_0$.

It is shown in the previous paper that the changes, $\Delta\mathbf{\Pi}'$ say, that are to be added to $\mathbf{\Pi}'$ for the blocking of 0 are given by

$$\Delta\mathbf{\Pi}' = \begin{bmatrix} 0 & 0_{(1,N-1)} \\ -\tilde{\boldsymbol{\pi}}_0' & \tilde{\mathbf{\Pi}}' \mathbf{J}^{-1} \mathbf{K} \tilde{\mathbf{R}}_0' \end{bmatrix} \tag{2}$$

where $\tilde{\mathbf{\Pi}}'$ is the $(N-1) \times \nu_0$ block of $\mathbf{\Pi}'$ with all rows except row 0 and only the columns indexed by indices in $\mathbf{N}_0$; symmetrically, $\tilde{\mathbf{R}}_0'$ is a $\nu_0 \times (N-1)$ block, $\mathbf{K}$ is a $\nu_0 \times \nu_0$ diagonal matrix, with ith diagonal element $p_{i0}' = p_{i0}$, since $\mathbf{P}$ and $\mathbf{P}'$ differ only in row 1; and, finally, the $\nu_0 \times \nu_0$ matrix $\mathbf{J}$ is given by

$$\mathbf{J} = \mathbf{I}_{\nu_0} - \mathbf{K} \hat{\mathbf{R}}_0' \tag{3}$$

where $\hat{\mathbf{R}}_0'$ is the $\nu_0 \times \nu_0$ block of $\mathbf{\Pi}'$ with both rows and columns indexed by indices in $\mathbf{N}_0$.

After the double operation of opening the new trap and blocking the old, the resulting matrix of expected numbers of visits can be denoted as $\mathbf{\Pi}''$, and it takes the form

$$\mathbf{\Pi}'' = \begin{bmatrix} 1 & 0 & 0_{(1,N-2)} \\ 0 & 1 & 0_{(1,N-2)} \\ 0_{(N-2,1)} & \iota_{(N-2,1)} & \tilde{\mathbf{\Pi}}'' \end{bmatrix}$$

where the forms of rows and columns 0 and 1 are dictated by the facts that 0 is a blocked site and that 1 is the sole trap open on the lattice. Plainly, all we need concern ourselves with is the $(N-2) \times (N-2)$ block $\tilde{\mathbf{\Pi}}''$. This block can be constructed by starting from the corresponding block of $\mathbf{\Pi}$ and adding the corresponding blocks of the two matrices of changes, $\Delta\mathbf{\Pi}$ and $\Delta\mathbf{\Pi}'$.

From eq 1, the appropriate block of $\Delta\mathbf{\Pi}$ is

$$-\frac{1}{\pi_{11}} \boldsymbol{\pi}_1 \boldsymbol{\rho}_1 \tag{4}$$

and, from eq 2, that of $\Delta\mathbf{\Pi}'$ is

$$\mathbf{L} \mathbf{J}^{-1} \mathbf{K} \mathbf{R} \tag{5}$$

where $\mathbf{L}$ and $\mathbf{R}$ are respectively $(N-2) \times \nu_0$ and $\nu_0 \times (N-2)$ blocks of $\mathbf{\Pi}'$. What we really want is an expression involving only blocks and elements of $\mathbf{\Pi}$, without the need to calculate $\mathbf{\Pi}'$ in an intermediate step. Given eq 1, $\mathbf{L}$ and $\mathbf{R}$ can be constructed as follows. Let $\boldsymbol{\pi}_i$ and $\boldsymbol{\rho}_i$ be respectively the ith

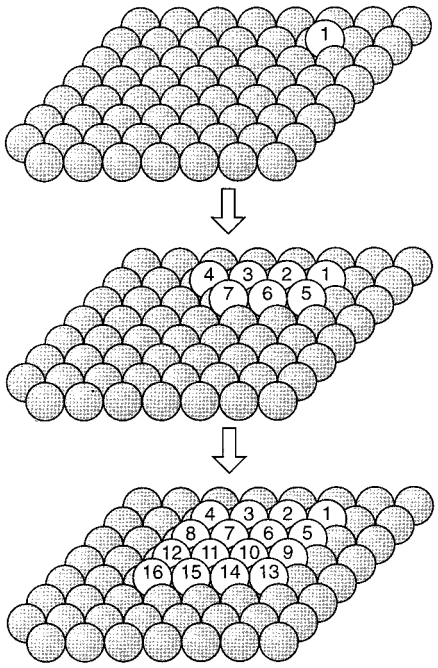

Figure 1. The "row filling" nucleation sequence.

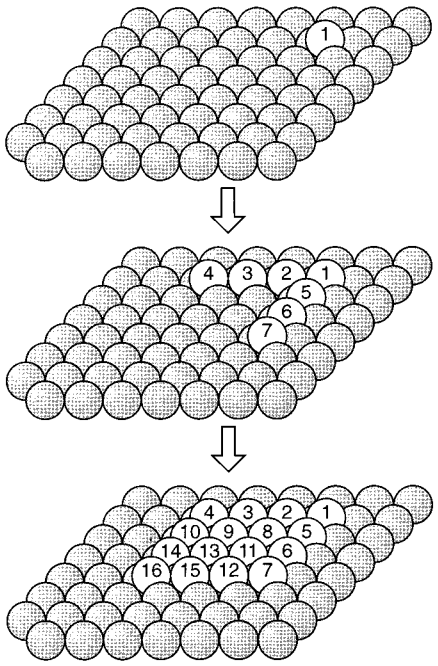

Figure 2. The "dendrite" nucleation sequence.

column and row of $\mathbf{\Pi}$. Then for $i \in \mathbf{N}_0$, the ith column of $\mathbf{L}$ is

$$\boldsymbol{\pi}_i - \frac{\pi_{1i}}{\pi_{11}}\boldsymbol{\pi}_1 \tag{6a}$$

but without rows 0 and 1, and the ith row of $\mathbf{R}$ is

$$\boldsymbol{\rho}_i - \frac{\pi_{i1}}{\pi_{11}}\boldsymbol{\rho}_1 \tag{6b}$$

without columns 0 and 1. The $\hat{\mathbf{R}}$ used in computing $\mathbf{J}$ in eq 3 can then be got by selecting ν_0 columns of $\mathbf{R}$, and $\mathbf{K}$ is defined directly in terms of the original $\mathbf{P}$ matrix. The changes to $\mathbf{\Pi}$ brought about by the double operation are then given by the sum of eqs 4 and 5 and can be computed directly from the original $\mathbf{P}$ and $\mathbf{\Pi}$ matrices.

III. Island Growth

We now take up the general question raised in the Introduction, namely, can one quantify the stochastic consequences of assuming different sequences in generating a given nucleation pattern or morphology on a finite planar array. To visualize the processes we wish to study, consider first the finite array sketched at the top of Figure 1. The shaded circles in this figure define atoms of the underlying substrate or host lattice; in this paper, we will consider arrays having both square planar and triangular symmetry, with the total number N of atoms defining the host lattice fixed at $N = 48$. Suppose now that a first atom, after deposition, diffuses randomly on this lattice and becomes immobilized in a certain location; the open circle labeled "one" in the display at the top of Figure 1 denotes such an adatom. The average number $\langle n\rangle_1$ of random displacements before immobilization (or "trapping") on a $N = 48$ lattice with square planar symmetry is $\langle n\rangle_1 = 94.295\,750$. Once this first adatom is locked in place, one can calculate the average number $\langle n\rangle_2$ of steps required for a second diffusing atom to be immobilized, but subject to the constraint that now one site is "blocked" or inaccessible to the second random walker; thus, the number N' of sites available to the second atom is $N' = N - 1 = 47$ and, using the method described in section II, we calculate $\langle n\rangle_2 = 95.033\,096$ before trapping on the same square planar lattice.

Recall that, in nucleation theory, the size at which for the first time an island becomes more stable with the addition of just one more atom[3−7] is defined as the critical island size i. Because we shall describe below the statistical consequences of continuing this process of sequential trapping, in effect $i = 1$ in this model calculation.

Referring again to Figure 1, the nucleation pattern after the deposition of 7 adatoms on the underlying lattice is depicted in the center illustration, and the pattern after deposition of 16 adatoms on the substrate is depicted at the bottom of the figure. Noting the order ($1 \rightarrow 2 \rightarrow 3 \rightarrow ... \rightarrow 16$) in which the 16 atoms are deposited sequentially, we refer to this case as the "row filling" case.

Two other nucleation sequences are displayed in Figures 2 and 3. That specified in Figure 2 we designate as the "dendrite" case and that in Figure 3 as the "compact" case. Values of $\langle n\rangle_j$ for these three cases for deposition in a square planar array are given in Table 1. Then, in Table 2, we list the $\langle n\rangle_j$ values for deposition in a triangular lattice array. The calculations reported in Tables 1 and 2 were carried out assuming that when a diffusing atom encounters a site on the boundary of the $N = 48$ host lattice, the diffusing atom moves away from that site in its next displacement. For comparison, one can also consider the possibility that the diffusing atom can remain at that same boundary site before moving away, and the results obtained imposing this alternative boundary condition are listed in Table 3 for deposition in a square planar array.

It is useful to characterize the three growth patterns illustrated in Figures 1−3 in terms of the average branch thickness b of a fractal island. In the "hit and stick," diffusion-limited-aggregation (DLA) model[8,9] (regime I fractal growth), $b = 1$. Experimentally,[10−15] deposition is characterized by wider branch thicknesses ($b \approx 4$); it has been suggested by Zhang, Chen, and Lagally[16] that this regime (II) of extended fractal growth can be understood if every adatom, upon reaching the edge of a developing island, can relax to the extent that it has found at least two nearest neighbors within the atoms belonging to the island. They note that this regime can be defined on a triangular

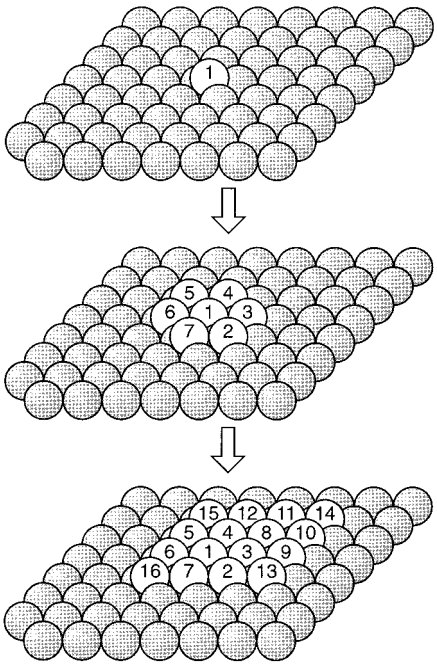

Figure 3. The "compact" nucleation sequence.

TABLE 1: Values of $\langle n \rangle_j$ for Three Nucleation Sequences Forming a 16 Atom Square-Planar Array

trap site	number of blocked sites	effective lattice size	row	dendrite	compact
1	0	48	94.295 750	94.295 750	58.480 519
2	1	47	95.033 906	95.033 906	70.427 292
3	2	46	93.240 683	93.240 683	130.589 08
4	3	45	100.895 93	100.895 93	85.475 202
5	4	44	91.157 266	91.157 266	89.158 769
6	5	43	113.088 78	83.323 382	130.574 60
7	6	42	107.651 52	86.545 244	139.159 66
8	7	41	104.271 11	124.320 39	127.140 26
9	8	40	83.280 712	106.030 66	107.090 15
10	9	39	102.512 49	96.205 496	151.452 74
11	10	38	95.862 836	111.349 25	123.677 53
12	11	37	90.260 874	94.035 788	148.570 80
13	12	36	83.427 533	101.431 89	135.046 22
14	13	35	99.766 017	86.556 127	193.746 68
15	14	34	91.970 378	91.970 378	124.176 20
16	15	33	84.268 109	84.268 109	84.268 109

lattice, but is absent on a square lattice. The center parts of Figures 1 and 2 are characterized by $b = 2$ and $b = 1$, respectively, and the bottom panel of all three figures is characterized by $b = 4$. In the following discussion, we shall discuss these different growth patterns, as well as developing branch thicknesses, from an entropic point of view.

IV. Discussion

We have reported calculations on a model designed to explore quantitatively the stochastic consequences of assuming different sequences for generating a given, final nucleation pattern or island morphology. In this concluding section, we link this discussion to the calculation of the entropic differences among the three nucleation schemes.

To begin, note that, as diagrammed, there are 16!/2! different ways in which the final morphology can be realized, so the cases considered here are only representative of the kind of efficiencies that can be gained (or not) when different assumptions are made on the cohesive energy among adatom species on a given lattice.

As a first step in understanding the results generated in this study, we plot $\langle n \rangle_j$ versus the number B of sites blocked in the nucleation process. Displayed in Figure 4 are the results obtained for deposition in a square-planar array for the "row filling" case and for the "compact" case. A similar plot is displayed in Figure 5 for deposition in a triangular array. For both symmetries, a pattern in the data emerges in the row filling case, namely, a systematic decrease in $\langle n \rangle_j$, once a given row has been initiated, followed by a "jump" in $\langle n \rangle_j$, once a given row has been filled and the next value of B is considered. More generally, one finds that for $B \geq 5$, values of $\langle n \rangle_j$ for the

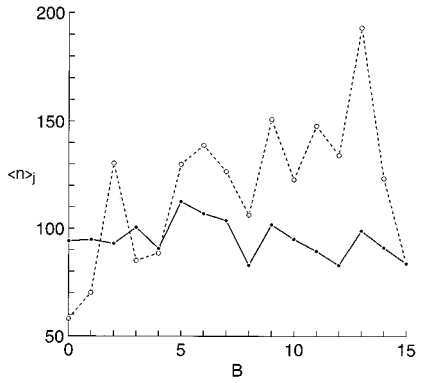

Figure 4. A plot of $\langle n \rangle_j$ versus the number B of blocked sites for a square-planar array. The "row filling" case is denoted by the solid line and the "compact" case by the dashed line.

TABLE 2: Values of $\langle n \rangle_j$ for Three Nucleation Sequences Forming a 16 Atom Triangular Array

trap site	number of blocked sites	effective lattice size	row	dendrite	compact
1	0	48	103.737 24	103.737 24	51.983 646
2	1	47	85.414 248	85.414 248	68.378 585
3	2	46	75.196 521	75.196 521	86.994 866
4	3	45	74.105 288	74.105 288	82.049 082
5	4	44	102.033 47	102.033 47	83.539 571
6	5	43	99.084 704	74.404 799	88.852 943
7	6	42	85.265 801	66.234 068	113.035 97
8	7	41	65.838 360	148.369 67	89.331 439
9	8	40	88.960 599	91.108 973	100.720 69
10	9	39	87.543 000	61.397 650	117.454 98
11	10	38	74.451 960	121.711 18	123.280 48
12	11	37	55.684 651	64.218 968	139.160 97
13	12	36	84.016 225	102.418 32	128.578 89
14	13	35	83.194 300	53.960 768	182.342 93
15	14	34	70.396 682	70.3966 81	117.573 98
16	15	33	52.677 996	52.677 996	52.6779 96

TABLE 3: Values of $\langle n \rangle_j$ for Three Nucleation Sequences Forming a 16 Atom Square-Planar Array with the Diffusing Atom Subject to Passive Boundary Conditions (See Text)

trap site	number of blocked sites	effective lattice size	row	dendrite	compact
1	0	48	108.182 17	108.182 17	68.135 65
2	1	47	109.986 95	109.986 95	82.042 055
3	2	46	108.405 07	108.405 07	152.634 81
4	3	45	117.537 06	117.537 06	100.811 25
5	4	44	108.078 55	108.078 55	105.696 42
6	5	43	136.479 90	99.751 864	155.372 50
7	6	42	130.484 48	104.156 27	166.150 48
8	7	41	126.240 07	154.098 19	152.740 17
9	8	40	101.614 04	132.340 59	128.938 16
10	9	39	127.693 11	120.188 99	183.083 50
11	10	38	120.310 12	140.830 89	150.682 76
12	11	37	113.577 26	119.554 19	182.980 99
13	12	36	105.133 17	130.413 91	167.592 27
14	13	35	128.670 27	112.183 15	238.562 51
15	14	34	119.998 27	119.998 27	157.127 25
16	15	33	110.947 50	110.947 50	110.947 50

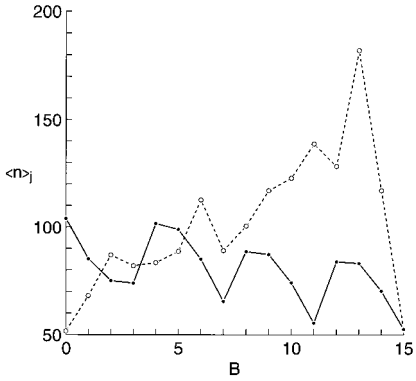

Figure 5. A plot of $\langle n \rangle_j$ versus the number B of blocked sites for a triangular array. The "row filling" case is denoted by the solid line and the "compact" case by the dashed line.

TABLE 4: Values of S_j/k for Three Nucleation Sequences Forming a 16 Atom Square-Planar Array

trap site	number of blocked sites	effective lattice size	row	dendrite	compact
1	0	48	5.683 817	5.683 817	5.221 501
2	1	47	5.700 362	5.700 362	5.407 232
3	2	46	5.685 875	5.685 875	6.028 048
4	3	45	5.766 754	5.766 754	5.613 250
5	4	44	5.682 858	5.682 858	5.660 571
6	5	43	5.916 177	5.602 686	6.045 825
7	6	42	5.871 254	5.645 892	6.112 894
8	7	41	5.838 185	6.037 590	6.028 738
9	8	40	5.621 182	5.885 379	5.859 333
10	9	39	5.849 630	5.789 065	6.209 942
11	10	38	5.790 073	5.947 560	6.015 177
12	11	37	5.732 483	5.783 770	6.209 382
13	12	36	5.655 228	5.870 713	6.121 534
14	13	35	5.857 253	5.720 133	6.474 631
15	14	34	5.787 477	5.787 477	6.057 056
16	15	33	5.709 057	5.709 057	5.709 057

"compact" case are systematically larger than for the "row filling" case and, concomitantly, the overall time scale associated with the development of the pattern in the "compact" case is longer than for the other two cases studied here.

For the discrete geometric distribution, the probability of a random walker being trapped in m steps is[17,18]

$$P_m = \frac{1}{\langle m \rangle}\left(1 - \frac{1}{\langle m \rangle}\right)^{m-1} \tag{7}$$

for which the first moment is the mean walk length $\langle m \rangle$. Given the above representation for P_m, the entropy

$$S_j = -k\sum_m P_m \ln P_m \tag{8}$$

can be calculated for each step j in the process, and the overall entropy change for a sequence involving r distinct precursor states is

$$\Delta S = S_f - \sum_{j=1}^{r} S_j = k\ln \frac{\langle m \rangle_f \, e^{-(r-1)}}{\langle m \rangle_1 \langle m \rangle_2 \ldots \langle m \rangle_r} \tag{9}$$

where S_f is the entropy associated with realizing the final state.

Displayed in Table 4 are the values of S_j/k for the three nucleation sequences studied here for the case of deposition in a square-planar array. Although the logarithmic dependence of S_j on the P_m suppresses the effects of differences in the calculated first moments $\langle m \rangle_j$, the data in Table 4 are consistent with the results diagrammed in Figures 4 and 5 in showing that for $j > 5$, the entropies calculated for the "compact" case are systematically larger than for the "row filling" and "dendrite" cases.

A further insight can be derived by recalling that for two uncoupled (independent) subsystems characterized by entropies S_1 and S_2, the entropy of the composite system is additive[19]

$$S = S_1 + S_2 \tag{10}$$

(even if the two systems are not at equilibrium), whereas if statistical independence is not satisfied,

$$S - (S_1 + S_2) < 0 \tag{11}$$

Hence, the presence of statistical correlations between two subsystems leads to an overall situation less random than when the systems are statistically independent of (or weakly coupled to) each other. The question then is, for which nucleation sequence are the statistical correlations most pronounced. Recall that the final pattern generated is the same in each case and that the last site filled in each nucleation sequence is the same; the state entropy S_{16}/k associated with that site ($j = 16$), as calculated using the result, eq 8, is determined to be 5.709 057. Adopting $j = 16$ as the final state of the system, the quantity

$$\Delta(S/k) = S_{16}/k - \sum_{j=1}^{15} (S_j/k) \tag{12}$$

can be calculated for each of the nucleation sequences considered here. The results are

$$\Delta(S/k)\ (\text{"row filling"}) = -80.729\ 551$$

$$\Delta(S/k)\ (\text{"dendrite"}) = -80.880\ 874$$

$$\Delta(S/k)\ (\text{"compact"}) = -83.356\ 057$$

Thus, the unfolding of the nucleation sequence defined by the "compact" case is characterized by a specificity which demands more significant statistical correlations between successive stages in the j-step process than the other two cases studied here.

Finally, we comment on the relevance of the calculations presented in this paper to the discussion in the review of Zhang and Lagally[1] on the manipulation of growth kinetics. A number of factors were identified that can influence the quality of $d = 2$ films grown by vapor-phase expitaxy: reduction in the island-edge barrier, hindering diffusion along island edges by impurities, increasing the island density, and enhancing atom mobility on top of an island with respect to that on the lower layers. Returning to Figures 4 and 5, and keeping in mind the relationship between the magnitude of $\langle n \rangle$ and the time scale of the process, we note that the values calculated for deposition in a square-planar array are systematically larger than the values calculated for deposition in a triangular array, regardless of the mechanism assumed (i.e., "row filling," "dendrite," or "compact"). We have already noted that of the two mechanisms, the $\langle n \rangle$-values for the "compact" mechanism are larger than the "row filling" mechanism, regardless of the lattice assumed. From these two observations, one can conclude that deposition in an array having square-planar symmetry via the "compact" mechanism requires the longest time to nucleate. Conversely, deposition in an array having triangular symmetry via the "row filling" mechanism requires the shortest time to nucleate. Thus, one may conclude that the most entropically favorable process for growth is one is which the morphology is generated by a "row filling" mechanism on lattices with triangular geometry

(e.g., on face-centered-cubic (fcc) (111) or hexagonal close-packed (hcp) (0001) substrates).

References and Notes

(1) Zhang, A.; Lagally, M. G. *Science* **1997**, *276*, 377.
(2) Davidson, R.; Kozak, J. J. *J. Phys. Chem.* **1998**, *102*, 7393.
(3) Mo, Y.-W.; Kleiner, J.; Webb, M. B.; Lagally, M. G. *Phys. Rev. Lett.* **1991**, *66*, 1998; *Surf. Sci.* **1992**, *268*, 275. Pimpinelle, A.; Villain, J.; Wolf, D. E. *Phys. Rev. Lett.* **1992**, *69*, 985.
(4) Vasek, J. E.; Zhang, Z. Y.; Salling, C. T.; Lagally, M. G. *Phys. Rev. B* **1995**, *51*, 17207. Quesenberry, P. E.; First, P. N. *Phys. Rev. B* **1996**, *54*, 8218.
(5) Andersohn, L.; Berke, Th.; Köhler, U.; Voigtländer, B. J. *Vac. Sci. Technol. A* **1996**, *14*, 312. Fehrenbacher, M.; Spitzmüller, J.; Memmert, U.; Rauscher, H.; Behm, R. J. *Vac. Sci. Technol.* 1499.
(6) Stroscio, J. A.; Pierce, D. T.; Dragoset, R. A. *Phys. Rev. Lett.* **1993**, *70*, 3615. Stroscio, J.; Pierce, D. *Phys. Rev. B* **1994**, *49*, 8522. Zuo, J.-K.; Wendelken, J. F.; Dürr, H.; Liu, C.-L. *Phys. Rev. Lett.* **1994**, *72*, 3064. Dürr, H.; Wendelken, J. F.; Zuo, J.-K. *Surf. Sci.* **1995**, *328*, L527.
(7) Brune, H.; Röder, H.; Boragno, C.; Kern, K. *Phys. Rev. Lett.* **1994**, *73*, 1955. Bott, M.; Hohage, M.; Morgenstern, M.; Michely, Th.; Comsa, G. *Phys. Rev. Lett.* **1996**, *76*, 1304.
(8) Witten, T. A.; Sander, L. M. *Phys. Rev. Lett.* **1981**, *47*, 1400.
(9) Meakin, P. *Phys. Rev. A* **1983**, *27*, 1495.
(10) Hwang, R. Q.; Schröder, J.; Günther, C.; Behm, R. J. *Phys. Rev. Lett.* **1991**, *67*, 3279.
(11) Michely, Th.; Hohage, M.; Bott, M.; Comsa, G. *Phys. Rev. Lett.* **1993**, *70*, 3943.
(12) Röder, H.; Hahn, E.; Brune, H.; Bucher, J.-P.; Kern, K. *Nature* **1993**, *366*, 141.
(13) Röder, H.; Bromann, K.; Brune, H.; Boragno, C.; Kern, K. *Phys. Rev. Lett.* **1995**, *74*, 3217.
(14) Hohage, M.; et al. *Phys. Rev. Lett.* **1996**, *76*, 2366.
(15) Brune, H.; et al. *Surf. Sci.* **1996**, *349*, L115.
(16) Zhang, Z. Y.; Chen, X.; Lagally, M. G. *Phys. Rev. Lett.* **1994**, *73*, 1829.
(17) Politowicz, P. A.; Kozak, J. J. *J. Phys. Chem.* **1990**, *94*, 7272.
(18) Abramowitz, M.; Stegun, I. A. *Handbook of Mathematical Functions*; Dover Publications: New York, 1972; Chapter 26.
(19) Wannier, G. H. Statistical Physics; Wiley: New York, **1966**.